END

DATE
FILMED

4 88

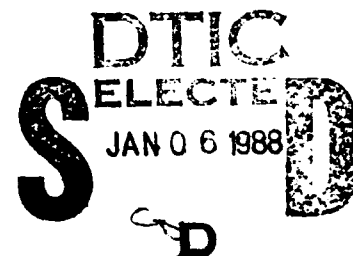ARL-AERO-PROP-R-174

AR-004-512

UTIC FILE COPY

DEPARTMENT OF DEFENCE

DEFENCE SCIENCE AND TECHNOLOGY ORGANISATION

AERONAUTICAL RESEARCH LABORATORIES

MELBOURNE, VICTORIA

Aero Propulsion Report 174

APPLICATION OF FINITE ELEMENT METHODS WITH
CYCLIC ELASTO-PLASTIC STRAIN ANALYSIS TO LOW
CYCLE FATIGUE ANALYSIS OF ENGINE COMPONENTS (U)

by

N.S. SWANSSON

DTIC
SELECTE
JAN 0 6 1988
D

Approved for Public Release

DECEMBER 1986

APPLICATION OF FINITE ELEMENT METHODS
WITH CYCLIC ELASTO-PLASTIC STRAIN ANALYSIS
TO LOW CYCLE FATIGUE ANALYSIS
# OF ENGINE COMPONENTS

by

N.S. SWANSSON

SUMMARY

Low Cycle Fatigue (LCF) in engine components involves macroscopic cyclic plastic strains (with a stress-strain hysteresis loop) over a significant portion of the failure region. Characterising elasto-plastic behaviour in potential failure regions is a necessary step in estimating LCF life.

The equations governing elasto-plastic behaviour are summarized, and the methods of implementing them in Finite Element (FE) stress analysis programs discussed.

An extension of the PAFEC program to include mixed isotropic-kinematic hardening is outlined, and verified by examples for which alternative FE solutions were available.

A sample application has been made to holes in a plate with biaxial stress fields similar to those in disc webs, and the results compared with the Neuber and modified Stowell rules commonly used for design life estimation; these rules tend to overestimate the strain in biaxial stress conditions, leading to conservative life estimates.
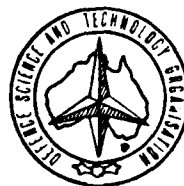
POSTAL ADDRESS: Director, Aeronautical Research Laboratories,
P.O. Box 4331, Melbourne, Victoria, 3001, Australia.

CONTENTS

A-1

DTIC
COPY
INSPECTED
6

NOTATION

General

A	area
c	kinematic hardening coefficient
E	Young's modulus
f	yield function
F	force
g, h	section dimensions
G	shear modulus
H	plastic slope
K	stress or strain concentration factor
M	moment
V	shear force
Vol	volume
r	radius or radial coordinate
s	arc distance
x	linear coordinate
u	displacement
α	rotation of face
β	rotation derivative
ϵ	strain
γ	shear strain
κ	shape coefficient for shear deflection
λ	proportionality constant
μ	kinematic hardening constant
ν	Poisson's ratio
ϕ	angular coordinate
ρ	isotropic fraction in mixed hardening
σ	stress
ω	total rotation

Tensors

C	elastic or plastic constitutive tensor
J	tensor invariant
s	deviatoric stress tensor
$\bar{s}$	translated stress deviator
α	translation of stress origin
δ	Kronecker delta
ϵ	strain tensor
σ	stress tensor

Matrices or Vectors

$\mathbf{B}$	strain – displacement transformation matrix
$\mathbf{D}$	stress – strain constitutive matrix
$\mathbf{F}$	load vector
$\mathbf{u}$	displacement vector
ϵ	strain vector
σ	stress vector

1

Subscripts or Superscripts

A   applied loads
E   elastic
P   plastic
y   current yield condition

1. INTRODUCTION

As engine power and speed is varied in an aircraft turbine engine, vital components are subject to changes in thermal and mechanical loading. Each flight includes one major start-stop cycle, plus lesser cycles depending on the manner of operation of the engine. High stress levels are used in many components to achieve lightness and consequent high specific output, and cyclic variation of stresses in the components leads ultimately to cracking at critical stress locations, with failure by the process of low cycle fatigue (LCF).

There are no practical or economic means of determining by inspection when the LCF life of components is exhausted, so accurate and reliable means of life estimation are needed. Three categories of data are required for LCF life prediction:

(i)   The loading history, preferably obtained from operational records for the engine, alternatively derived from simulation or estimates.

(ii)   Modelling and analytical methods which use the operational loading to produce the history of stress, strain (and temperature where relevant) at critical locations in components where failure may originate.

(iii)   A damage accumulation criterion, so the cumulative effect of loading cycles can be quantified and a measure of fatigue damage provided. This may be related either to the life to crack initiation (for safe life estimates), or to estimated crack propagation rate (in damage tolerant design using fracture mechanics methods).

Thermodynamic and heat flow analyses of engine operational data are used to de-.ermine generalised loadings, including pressures, metal temperatures and rotor speeds. Finite element (FE) models handle the complex boundary shapes commonly found in practical components, so FE computer programs are generally used for determination of detailed temperature, stress and strain distributions.

Since LCF by definition is characterised by macroscopic cyclic plastic strains manifested by a stress-strain hysteresis loop over a significant portion of the failure region, a material model incorporating cyclic plastic behaviour is required. Predicted stress and strain values depend on plastic properties of the material. Further, when the component is unloaded, plastic behaviour leaves residual stresses which also influence fatigue life.

High cycle fatigue life predictions are based on elastic stress estimates (Basquin law), but strain amplitude is regarded as the best parameter for predicting LCF life. Total strain values (elastic plus plastic) are used in the Coffin-Manson equation[1], adopted almost universally for LCF prediction. Hence characterising elasto-plastic behaviour in potential failure regions is a necessary step in estimating LCF life.

This report summarises the equations governing elasto-plastic behaviour, indicates how they are implemented in FE stress analysis programs, evaluates and compares FE packages available at ARL, describes the extension of the PAFEC program at ARL to include mixed isotropic-kinematic hardening, and gives applications of FE elasto-plastic analysis under loading resembling engine components, comparing results with the commonly used Neuber and Stowell approximations.

2. CYCLIC PLASTICITY ANALYSIS

In addition to equilibrium and compatibility (strain-displacement) relations used in elastic stress analysis (and not changed in form if strains are assumed to be small), three concepts are required to formulate cyclic plasticity problems[2].

(i)   Initial Yield Criterion

A number of yield criteria[3,4] have been formulated, but only the maximum shear of Tresca, and the distortion energy or octahedral shear of von Mises are used for normal

3

ductile metals. For the more commonly used materials the von Mises criterion agrees better with test data, and is mathematically simpler as it defines a single continuous failure surface. This surface is expressed in terms of a function of the second invariant $(J_2 = s_{ij} s_{ij})$ of the deviatoric stress tensor s_{ij} and can be written:

$$f = (\frac{3}{2} s_{ij} s_{ij})^{\frac{1}{2}} - \sigma_0 = 0$$

where σ_0 is the initial yield stress in uniaxial tension
$s_{ij} = \sigma_{ij} - \delta_{ij} \sigma_{kk}/3$, with stress tensor σ_{ij} and Kronecker delta δ_{ij}
$\sigma_{kk} = \sigma_{11} + \sigma_{22} + \sigma_{33}$, using the tensor convention that repeated dummy
subscripts indicate summation

In 3-dimensional principal stress space, the von Mises criterion describes a cylindrical surface, of radius $\sigma_0 = (\frac{3}{2} s_{ij} s_{ij})^{\frac{1}{2}}$ with axis through the origin and equally inclined to the three principal stress axes (Fig. 1). For plane stress ($\sigma_3 = 0$), this surface intersects the σ_1, σ_2 principal stress plane in an ellipse.

(ii)   Plastic Flow Law

Total increments in strain are assumed to be divisible into elastic and plastic fractions:

$$d\epsilon_{ij} = d\epsilon_{ij}^E + d\epsilon_{ij}^P$$

The direction of the plastic strain increment tensor, according to the associated flow rule, is normal to the yield surface (requiring maximum plastic work on deformation):

$$d\epsilon_{ij}^P = d\lambda \frac{\partial f}{\partial \sigma_{ij}}$$

where $d\lambda$ is a constant of proportionality. This is the normality condition and for a von Mises material, is equivalent to the Prandtl-Reuss equations $d\epsilon_{ij}^P = d\lambda \, s_{ij}$.

(iii)   Strain Hardening Rule

In many materials yield strength increases progressively with increasing plastic strain. While the von Mises yield criterion and the normality flow rule for plastic strain are generally accepted and adequately established by experiment, a similar consensus does not exist for rules used to describe strain hardening. Simpler rules are preferred, provided their behavioural description is reasonable, as more elaborate hardening models lead to considerable complexity in finite element programs. Four main hardening rules have been used, viz. isotropic, kinematic, Mroz or multiple surface models, and sublayer or subvolume models.

(a)   Isotropic Hardening

The simplest assumption is that material strengthens uniformly with increasing plastic strain, irrespective of strain direction   forward and reversed loading have equal effects (Fig. 2). This implies that the yield surface radius expands uniformly in stress space, maintaining shape, orientation, and origin of axis (Fig. 3). Isotropic hardening does not satisfactorily model reversed or cyclic loading, but its implementation is simple and for monotonic loading results are as good as for more complex models[5] .

(b)   Kinematic Hardening

When loading is reversed, most metals exhibit a reduced yield strength in the reverse direction, known as the Bauschinger effect (Fig. 2). The kinematic hardening

4

model formulated by Prager[6] represents this effect by assuming that the yield surface translates as a rigid body in stress space, maintaining its size, shape, and orientation (Fig. 4). This translation, $d\alpha_{ij}$ is in the direction of the plastic strain increment, i.e. normal to the yield surface. The Prager formulation is not invariant in a subspace of reduced dimensions – it must be modified for a two dimensional system. Ziegler[15] formulated an alternative definition of the yield surface translation, $d\alpha_{ij}$ namely, that its direction is the vector connecting the centre point (or origin) of the current yield surface to the existing stress point. In most problems, the difference in the results from the Prager and Ziegler formulations is negligible, with the Prager equations generally more convenient to use. Both satisfactorily model reversed loading with elastic-perfectly plastic behaviour, or when the degree of strain hardening is limited, and hardening is reasonably linear. Difficulties arise at large reversed strains when the stress–strain relation for the material is highly nonlinear, because there is no satisfactory rule for relating hardening coefficient to cumulative strain.

(c)   Mixed Isotropic-Kinematic Hardening

Mixed hardening formulations[7,8] have been developed combining isotropic and kinematic hardening, which means that the yield surface both expands and translates. By extending the scope of the kinematic model, better agreement with test data is obtained for some materials. A particularly simple and readily implemented formulation of mixed hardening has been developed and is presented below.

(d)   Multi-Surface Models

Non-linear hardening, reduced in the uniaxial case to a piecewise linear stress–strain curve, is represented by the Mroz and subvolume models. The Mroz model[9] comprises a series of (initially concentric) yield surfaces, each related to a particular yield stress corresponding to one segment of the curve. When plastic strain occurs, the surface translates until it touches the next bounding surface, which is translated in turn. Contact between the surfaces is maintained until unloading occurs (Fig. 5).

A similar piecewise linear modelling is achieved by the sublayer or subvolume models[10,11]. These postulate that the material comprises a number of subvolumes (physically analogous to material grain structure). Each subvolume has elastic-perfectly plastic properties with a different yield stress. All are subject to the same strain, with their individual stresses combining to give total stress.

The Mroz and subvolume models result in the Masing description[12] of the Bausch-inger effect, viz. that on reversed loading the shape of initial loading curve is maintained, magnified by a factor of two. This is a satisfactory representation for many engineering materials. More elaborate models[13,14,23] have been formulated to describe fine details of behaviour, but generally these are too complex to implement in a finite element computer program, or too restricted in the materials represented.

3.   PLASTICITY EQUATIONS

Failure Criterion

A general form of the von Mises yield criterion, incorporating the various hardening rules, can be expressed as:

$$f = (\frac{3}{2}\bar{s}_{ij}) - \sigma_s(\epsilon^P) = 0 \qquad (1)$$

where
$$\bar{s}_{ij} = s_{ij} - \alpha_{ij} \qquad (2)$$

5

and $s_{ij} = \sigma_{ij} - \delta_{ij}\sigma_{kk}/3$ as previously defined. $\sigma_s(\epsilon^P)$ is the yield stress as a function of the plastic strain. The translation α_{ij} of the stress origin is also a function of plastic strain, depending on the hardness model adopted, and determines $\bar{s}_{ij}$, the translated deviatoric stress.

Plastic Flow Equations

Strain Partitioning

$$d\epsilon_{ij} = d\epsilon_{ij}^E + d\epsilon_{ij}^P \tag{3}$$

Normality Condition

$$d\epsilon_{ij}^P = d\lambda \frac{\partial f}{\partial \sigma_{ij}} = \frac{3}{2}\frac{\bar{s}_{ij}}{\sigma_s}d\lambda \tag{4}$$

The proportionality constant $d\lambda$ is found by taking the inner product of equation (4):

$$\frac{2}{3}d\epsilon_{ij}^P d\epsilon_{ij}^P = \frac{3}{2}\frac{d\lambda^2}{\sigma_s^2}\bar{s}_{ij}\bar{s}_{ij}$$

so:
$$d\lambda = (\frac{2}{3}d\epsilon_{ij}^P d\epsilon_{ij}^P)^{\frac{1}{2}} = d\epsilon^P \tag{5}$$

For a von Mises material $d\lambda = d\epsilon^P$ is equal to the strain in uniaxial tension.

Strain Hardening

Isotropic $\alpha_{ij} = 0$
$$d\sigma_s = H d\epsilon^P$$
where H is the plastic slope in simple tension, so $\sigma_s = \sigma_y$, the yield stress in tension.

Kinematic $d\sigma_s = 0$ so $\sigma_s = \sigma_0$, the initial yield stress.
$$d\alpha_{ij} = c\,d\epsilon_{ij}^P \qquad \text{(Prager)}$$
$$d\alpha_{ij} = d\mu(\sigma_{ij} - \alpha_{ij}) \qquad \text{(Ziegler)}$$

Equivalence with uniaxial tension requires that the constants $c = \frac{2}{3}H$, or $d\mu = \frac{H}{\sigma_s}d\epsilon^P$ so with equations (4) and (5):

$$d\alpha_{ij} = \frac{\bar{s}_{ij}}{\sigma_s}H\,d\epsilon^P \qquad \text{(Prager)} \tag{6}$$

or:
$$d\alpha_{ij} = \frac{\sigma_{ij} - \alpha_{ij}}{\sigma_s}H\,d\epsilon^P \qquad \text{(Ziegler)} \tag{7}$$

Mixed Hardening

The hardening effect $H\,d\epsilon^P$ in equations for isotropic and kinematic hardening can be divided into fractions ρ defining yield surface expansion (isotropic), and $(1-\rho)$ yield surface translation (kinematic). Notionally either the strain hardening rate H or the plastic strain increment $d\epsilon^P$ can be so partitioned, and this makes subsequent implementation in computer code particularly straightforward.

$$d\sigma_s = \rho H d\epsilon^P \tag{8}$$

so:
$$\sigma_s = \sigma_0 + \rho(\sigma_y - \sigma_0)$$

$$d\alpha_{ij} = \frac{s_{ij}}{\sigma_s}(1-\rho)H d\epsilon^P \qquad \text{(Prager)} \tag{9}$$

6

$$\epsilon : \quad d\alpha_{ij} = \frac{\sigma_{ij} - \alpha_{ij}}{\sigma_e}(1-\rho)H\,d\epsilon^P \quad \text{(Ziegler)}$$

Constitutive Equations

Constitutive equations relating increments of stress and elastic strain, using equation (3), can be written:

$$d\sigma_{ij} = C^E_{ijkl}\,d\epsilon^E_{kl} = C^E_{ijkl}\left(d\epsilon_{kl} - d\epsilon^P_{kl}\right) \tag{10}$$

where the elastic stiffness tensor is:

$$C^E_{ijkl} = 2G\left(\delta_{ik}\delta_{jl} + \frac{\nu}{1-2\nu}\delta_{ij}\delta_{kl}\right)$$

with shear modulus G, Poisson's ratio ν.

Constitutive equations for plastic deformation are derived by noting that during plastic flow the stress point stays on the yield surface, so that $df = 0$ in equation (1):

$$df = \frac{\partial f}{\partial \sigma_{ij}}d\sigma_{ij} + \frac{\partial f}{\partial \alpha_{ij}}d\alpha_{ij} + \frac{\partial f}{\partial \sigma_e}d\sigma_e = 0 \tag{11}$$

Substituting in equation (1) and using (2), (8) and the Prager result of (9):

$$\frac{3}{2}\frac{\bar{s}_{ij}}{\sigma_e}\left(d\sigma_{ij} - d\alpha_{ij}\right) - \rho H d\epsilon^P = 0$$

$$\frac{3}{2}\frac{\bar{s}_{ij}}{\sigma_e}\left\{d\sigma_{ij} - (1-\rho)\frac{\bar{s}_{ij}}{\sigma_e}Hd\epsilon^P\right\} - \rho H d\epsilon^P = 0$$

with equations (3) and (10):

$$\frac{3}{2}\frac{\bar{s}_{ij}}{\sigma_e}C^E_{ijkl}\left\{d\epsilon_{kl} - \frac{3}{2}\frac{\bar{s}_{kl}}{\sigma_e}\right\}d\lambda - Hd\lambda = 0 \tag{12}$$

Since $\bar{s}_{ii} = 0$, for an elastically isotropic material only the "diagonal" components $i = k, j = l$ of the tensor C^E_{ijkl} produce non-zero terms, and equation (12) can be reduced to:

$$d\lambda = \frac{\bar{s}_{kl}\,d\epsilon_{kl}}{\sigma_e(1 + H/3G)} \tag{13}$$

Using equations (4) and (13) with (10), with dummy subscripts k,l changed to m,n:

$$d\sigma_{ij} = C^E_{ijkl}\left\{d\epsilon_{kl} - \frac{3}{2}\frac{\bar{s}_{kl}\bar{s}_{mn}\,d\epsilon_{mn}}{\sigma_e^2(1 + H/3G)}\right\}$$

$$d\sigma_{ij} = (C^E_{ijkl} - C^P_{ijkl})d\epsilon_{kl} \tag{14}$$

By a reduction similar to equation (13), the plastic constitutive tensor becomes:

$$C^P_{ijkl} = \frac{3G}{1 + H/3G}\frac{\bar{s}_{ij}\bar{s}_{kl}}{\sigma_e^2} \tag{15}$$

7

4. FINITE ELEMENT IMPLEMENTATION

Finite Element Analysis

For a continuum, the constitutive equation (14) can be used in standard finite element equations of incremental form. Using matrix notation:

$$\int \mathbf{B}^T (\mathbf{D} - \mathbf{D}^P) \mathbf{B} \, dVol \, \delta\mathbf{u} = \delta\mathbf{F}_A \tag{16}$$

$$(\mathbf{K} - \mathbf{K}^P) \delta\mathbf{u} = \delta\mathbf{F}_A \tag{17}$$

where $\mathbf{K}, \mathbf{K}^P$ are elastic and plastic structural stiffness matrices
$\delta\mathbf{F}_A$ is vector of applied loads
$\mathbf{B}$ is displacement strain transformation matrix so $\delta\epsilon = \mathbf{B} \, \delta\mathbf{u}$
$\mathbf{D}, \mathbf{D}^P$ are material elastic and plastic constitutive matrices,
corresponding to tensors C_{ijkl}^E, C_{ijkl}^P in equation (14).

Equation (17) provides an incremental solution for $\delta\mathbf{u}$ using the tangential stiffness matrix $(\mathbf{K} - \mathbf{K}^P)$. Because $\mathbf{K}^P$ is a function of stress, the solution is obtained by successive Newton-Raphson approximations, and the stiffness matrix has to be re-evaluated and reduced at each iteration.

Repeated matrix reductions can be avoided by re-arranging equation (16) so that only the constant elastic matrix $\mathbf{K}$ need be decomposed, which is required once only during the solution:

$$\int \mathbf{B}^T \mathbf{D} \, \mathbf{B} \, dVol \, \delta\mathbf{u} = \delta\mathbf{F}_A + \int \mathbf{B}^T \mathbf{D}^P \mathbf{B} \, dVol \, \delta\mathbf{u} \tag{18}$$

$$\mathbf{K} \, \delta\mathbf{u} = \delta\mathbf{F}_A + \delta\mathbf{F}_P \tag{19}$$

The plastic pseudo-forces $\delta\mathbf{F}_P$ are found by noting that when equations (10) and (14) are written in matrix form:

$$\delta\boldsymbol{\sigma} = (\mathbf{D} - \mathbf{D}^P)\delta\epsilon = \mathbf{D}(\delta\epsilon - \delta\epsilon_P) \tag{20}$$

Hence $\mathbf{D}^P \delta\epsilon = \mathbf{D} \, \delta\epsilon_P$ and since $\delta\epsilon = \mathbf{B} \, \delta\mathbf{u}$ the RHS integral in equation (18) becomes:

$$\delta\mathbf{F}_P = \int \mathbf{B}^T \mathbf{D} \, dVol \, \delta\epsilon_P \tag{21}$$

Partitioning $\delta\mathbf{u} = \delta\mathbf{u}_E + \delta\mathbf{u}_P$ in equation (19) leads to:

$$\mathbf{K}(\delta\mathbf{u}_E + \delta\mathbf{u}_P) = \delta\mathbf{F}_A + \delta\mathbf{F}_P \tag{22}$$

The equation $\mathbf{K} \, \delta\mathbf{u}_E = \delta\mathbf{F}_A$ is simply a scaled elastic solution which can be subtracted from equation (22) giving:

$$\mathbf{K} \, \delta\mathbf{u}_P = \delta\mathbf{F}_P \tag{23}$$

In this equation $\delta\mathbf{u}_P$ is found by iterative solution, with successive approximations to $\delta\mathbf{F}_P$ given by equation (21).

Computer Programs

The commercial FE program package PAFEC was available at ARL as a general purpose stress analysis, heat flow and dynamics program when this work commenced.

Subsequently access to NASTRAN was acquired for special applications, and the plasticity capabilities of both program packages are now briefly compared.

PAFEC uses the development just presented; a flow chart of the PAFEC plasticity routine is shown in Figure 6. This approach is simple, but at times it results in convergence difficulties. NASTRAN by comparison uses the tangential stiffness approach of equation (17), though a flexible strategy is employed by updating the matrix only after an optimum number of iterations. Convergence is assured, but computational effort is greater.

Regarding types of elements available for elasto-plastic problems, PAFEC is much more versatile, and NASTRAN is highly restricted in its ability to model continua of complex shape, typical of aircraft engine components. For 2-dimensional models, NASTRAN has only straight-sided linear elements, with plastic conditions represented only at the centroid. In three dimensions more capability is offered by linear brick elements with $2 \times 2 \times 2$ Gauss point integration, and equivalent triangular prism elements. By comparison PAFEC has, as well as linear elements, quadratic and cubic isoparametric elements in two and three dimensions, with 2×2 or $2 \times 2 \times 2$ Gauss integration. Both triangular and rectangular (or brick and prism) shapes are available, and the curved shapes obtainable with isoparametric elements allow better modelling of practical components.

Hardening rules available are similar. Both programs have isotropic and kinematic models. NASTRAN also offers "mixed" hardening, but this is restricted to the special case of $\rho = 0.5$ in equations (8) and (9), which implies that the yield stress always remains equal to the initial value despite reversal of loading. The writer has extended PAFEC code to incorporate the more general case of mixed hardening described by these equations. Nonlinear hardening is available with the isotropic model, but with kinematic hardening PAFEC expresses the yield surface translation in an equation of the form $\alpha_{ij} = \frac{2}{3} H \epsilon_{ij}^{P}$, which requires constant H (i.e. linear hardening) when integrating equation (6).

5. COMPARISON OF SOLUTIONS

As a preliminary to using PAFEC in practical analysis of cyclic plasticity, suitable verification problems were sought. The only reasonably accessible example which included linear strain hardening, was the proving ring problem in [9] ; an alternative solution to this problem showing slightly different results is also found in [15]. The same problem with mixed hardening is treated in [7] . The proving ring and its material properties are shown in Figure 7, and preliminary results with PAFEC level 5.2 are shown in Figure 8.

The initial results reveal significant discrepancies, and when after discussion no satisfactory reason could be found [16], a detailed examination of PAFEC code was undertaken. Various differences between implemented code and plasticity equations were found (listed in Appendix B), most of them having only minor effects on results. However changes in the way of satisfying convergence, either by imposing stricter requirements, or by adopting a self-correcting scheme [17,18], produced significant changes in results for this problem. It is expected that updated levels of PAFEC code will incorporate appropriate modifications [16] .

Alternative FE programs such as NASTRAN were not accessible at ARL at this time, and no satisfactory published results for suitable test cases were available. So in order to test the modifications, original theoretical solutions were developed for test problems, given in Appendix A. Starting with the simple case of a rectangular beam in

pure bending, solutions are extended to a curved rectangular bar in pure bending, and finally the proving ring which is a curved bar under both bending and tension.

Results for the straight beam and curved bar in pure bending are shown in Figure 9, and for the proving ring in Figure 8. In all cases excellent agreement is obtained between the modified PAFEC and the theoretical solutions. NASTRAN had by this time become available at ARL, so it was used for the proving ring, giving a solution virtually coincident with modified PAFEC.

Cyclic loading for the proving ring is shown in Figure 10, comparing isotropic, kinematic and mixed hardening (for $\rho = 0.25$), with results qualitatively similar to those given in [6] .

6. APPLICATION AND DISCUSSION

Simple semi-empirical rules for dealing with plastic deformation at stress concentrations when the plastic properties of the material are known, have been developed by extending solutions obtained for particular geometries to more general cases. At a notch root with shear stresses, Neuber[23] derived the relation:

$$K_t^2 = K_\sigma K_\epsilon \qquad \text{or} \qquad K_\epsilon = \frac{K_t^2}{K_\sigma} \qquad (24)$$

where K_t = theoretical elastic stress concentration factor

K_σ = stress factor $\sigma/\bar{\sigma}$

K_ϵ = strain factor $\epsilon/\bar{\epsilon}$

Stowell[24] obtained a series solution for elasto plastic deformation around a hole in an infinite plate under uniaxial stress, which when modified to cover general stress concentrations [25] is expressed:

$$K_\epsilon = (K_t - 1)\frac{K_\sigma}{K_\sigma - 1} \qquad (25)$$

Compressor and turbine discs subject to rotational, other mechanical and possibly also thermal loading are generally the most critical aircraft engine components subject to low cycle fatigue. A major failure source is at holes in the disc web, where stress conditions surrounding the hole are substantially biaxial.

For a circular hole in an infinite thin plate, where stress conditions resemble those in a turbine disc, finite element, Neuber and modified Stowell solutions are compared. Principal stress ratios $\sigma_2/\sigma_1 = 0$ (uniaxial), 0.5 and 1.0 (pure biaxial) are shown in Figures 11, 12 and 13 respectively. Little difference between the three stress solutions can be seen, largely because of the low plastic hardening slope (typical Ti-8-1-1 material properties were used). Strain solutions differ significantly, depending on the principal stress ratio. For uniaxial stress ($\sigma_2 = 0$, $K_t = 3.0$), the modified Stowell and finite element solutions coincide, at least for lower values of plastic strain (as would be expected, since the Stowell equation derives from a series solution for this case). As stress increases, the Stowell equation tends to overestimate strain, and the Neuber solution is similar, excepting that it overestimates strain throughout the stress range.

As stresses become more nearly biaxial, both Neuber and modified Stowell rules continue to overestimate strain. With pure biaxial stresses ($\sigma_2 = \sigma_1$, $K_t = 2.0$), Neuber and Stowell give similar moderate overestimates at low plastic strains, with Stowell giving much higher excess estimates of strain at higher stresses. Fortunately such estimates lead to conservative LCF life predictions when using the Coffin Manson law.

10

The limitations of the Neuber and modified Stowell rules have been considered elsewhere[21] . Generally speaking they overpredict plastic strain, but this depends on the particular geometry. Most investigations have been concerned with their accuracy for LCF fatigue life prediction[19],[20] rather than for strain estimation, and in this respect they are widely accepted as useful design rules.

A thin disc with negligible stresses through its thickness has been assumed in the current analysis, and the effect of biaxial stresses in the thickness direction at the hole surface has not been considered. With surface biaxial stresses a correction should be applied[21] , which tends to reduce predicted strains. The preliminary applications described herein are intended to be followed by a fuller explorations of thick discs, plastic crack growth and other practical LCF applications in the next phase of this investigation.

7. CONCLUSIONS

Application of PAFEC to cyclic elasto–plastic calculation has been established at ARL. Careful investigation after finding discrepancies between results and published solutions led to the development and verification of modified code. This code extended the available strain hardening models by adding mixed hardening, for which a simple formulation was developed, to the existing isotropic and kinematic hardening rules. Verification entailed the determination of original alternative solutions to problems of bending and stretching of straight and curved bars, the latter exemplified by a proving ring for which several alternative FE solutions were available.

Sample applications were made to holes in plates with biaxial stress similar to disc webs, and results compared with the Neuber and modified Stowell rules, commonly used for design life estimation. Compared with finite element solutions, these rules tend to overestimate strain in biaxial stress conditions, which would lead to a conservative life estimate.

A further complexity ensues when the disc or plate is of sufficient thickness that stress levels are significant in the thickness direction. Stress conditions at the hole surface are then biaxial, and corrections need to be applied to give equivalent uniaxial strains. Multiaxial fatigue is a complex topic and is not considered here; it has been addressed in numerous papers elsewhere[26] . Practical discs generally exhibit biaxial and often triaxial effects, and analysis of these discs is proposed in the next phase of this work.

REFERENCES

1. **Coffin,L.F.Jr.** (1974) "Fatigue at High Temperature – Prediction and Interpretation" *Proc.I.Mech.E.*, *Vol.188, p.109*

2. **Kalev,I.** (1981) "Cyclic Plasticity Models and Application in Fatigue Analysis" *Computers & Structures Vol.13 p.709*

3. **Nayak,G.C. & Zienkiewicz,O.C.** (1972) "Elasto-Plastic Stress Analysis. A Generalisation for Various Constitutive Relations Including Strain Softening" *Int.J.Num.Meth.Eng. Vol.5 p.113*

4. **Marques,J.M.M. & Owen,D.R.J.** (1984) "Some Reflections on Elastoplastic Stress Calculation in Finite Element Analysis" *Computers & Structures Vol.18 p.1135*

5. **Hunsaker,B.Jr., Vaughan,D.K., Stricklin,J.A. & Haisler,W.A.** (1973) "A Comparison of Current Work Hardening Models Used in the Analysis of Plastic Deformations" *Texas Engineering Experiment Station AD-776667*

6. **Prager,W.** (1955) "The Theory of Plasticity: A Survey of Recent Achievements" *Proc.I.Mech.E. Vol.169 p.41*

7. **Axelsson,K. & Samuelsson,A.** (1979) "Finite Element Analysis of Elastic-Plastic Materials Displaying Mixed Hardening" *Int.J.Num.Meth.Eng. Vol.14 p.211*

8. **Sowerby,R. & Tomita,Y.** (1977) "On the Bauschinger Effect and its Influence on the U.O.E. Pipe Making Process" *Int.J.Mech.Sci. Vol.19 p.351*

9. **Mroz,Z.** (1969) "An Attempt to Describe the Behaviour of Metals under Cyclic Loads Using a More General Work-Hardening Model" *Acta Mechanica Vol.7 p.199*

10. **Owen.D.R.J., Prakash,A. & Zienkiewicz,O.C.** (1974) "Finite Element Analysis of Non-Linear Composite Materials by Use of Overlay Systems" *Computers & Structures Vol.4 p.1251*

11. **McKnight,R.L. & Sobel,L.H.** (1977) "Finite Element Cyclic Thermoplasticity by the Method of Subvolumes" *Computers & Structures Vol.7 p.189*

12. **Masing,G.** (1926) "Eigenspannungen und Verfestigung beim Messing" *Proc.2nd.Int. Cong.App.Mech. p.322*

13. **Asaro,R.J.** (1975) "Elastic-Plastic Memory and Kinematic Type Hardening" *Acta Metallurgica Vol.23 p.1255*

14. **Popov,E.P. & Petersson,H.** (1978) "Cyclic Metal Plasticity: Experiments and Theory" *Proc.ASCE J.Eng.Mech.Div. No.EM4 p.1371*

15. **Ziegler,H.** (1958) "A Modification of Prager's Hardening Rule" *Quart.App.Math. Vol.17 p.55*

16. **Owen,D.R.J. & Salonen,E.M.** (1975) "Three Dimensional Elasto-Plastic Finite Element Analysis" *Int.J.Num.Meth.Eng. Vol.9 p.209*

17. **Platt,J.** (1985) Private Communications re PAFEC

18. **Stricklin,J.A., Haisler,W.E. & von Riesemann,W.A.** (1971) "Geometrically Nonlinear Structural Analysis by Direct Stiffness Method" *Proc.ASCE J.Struct.Div No.ST9 p.2299*

19. **Hofmeister,L.D., Greenbaum,G.A. & Evensen,D.A.** (1971) "Large Strain Elasto Plastic Finite Element Analysis" *AIAA Journ. Vol.9 p.1248*

20. **Wundt,B.M.** (1972) "Effects of Notches on Low-Cycle Fatigue" *ASTM STP 490*

21. **Leis,B.N., Gowda,C.V.B & Topper,T.H.** (1973) "Cyclic Inelastic Deformation and the Fatigue Notch Factor" *Cyclic Stress Strain Behaviour — Analysis, Experimentation and Failure Prediction ASTM STP 519 p.133*

12

22. **Mowbray,D.F. & McConnelee,J.E.** (1973) "Applications of Finite Element Stress Analysis Techniques and Stress-Strain Properties in Determining Notch Fatigue Specimen Deformation and Life" *ibid. p.151*

23. **Jhansale,H.R. & Topper,T.H.** (1973) "Engineering Analysis of the Inelastic Stress Response of a Structural Metal under Variable Cyclic Strains" *ibid. p.246*

24. **Neuber,H.** (1961) "Theory of Stress Concentrations for Shear Strained Prismatical Bodies with Arbitrary Nonlinear Stress Strain Law" *Trans.ASME J.App.Mech. Vol.28 p.544*

25. **Stowell,E.Z.** (1950) "Stress and Strain Concentration at a Circular Hole in a Infinite Plate" *NACA Tech. Note 2073*

26. **Hardrath,H.F. & Ohman,L.** (1953) "A Study of Elastic and Plastic Stress Concentration Factors Due to Notches and Fillets in Flat Plates" *NACA Rept. 1117*

27. **Beaver,P.W.** (1984) "Multiaxial Fatigue and Fracture - A Literature Review" *Dept. of Defence, ARL Struc-R-410*

APPENDIX A – STRAIGHT AND CURVED BARS

Pure Bending of Straight Rectangular Bar

Adopting the standard beam assumption that plane sections remain plane, and using notation as in Figure 14, strains are given by:

$$\epsilon = \epsilon_{max}\frac{2x}{h} \quad \text{and} \quad \frac{g}{h} = \frac{\epsilon_y}{\epsilon_{max}}$$

if the elastic region is of depth g, yield strain ϵ_y. Stress-strain relations for a bilinear material with elastic modulus E, total plastic modulus H are:

$$-\epsilon_y \leq \epsilon \leq \epsilon_y \qquad \sigma = E\epsilon \tag{26}$$

$$\left.\begin{array}{c} \epsilon > \epsilon_y \\ \epsilon < -\epsilon_y \end{array}\right\} \qquad \sigma = (E - H)\epsilon_y + H\epsilon \tag{27}$$

Moment M per unit width of bar is:

$$M = 2\int_0^{\frac{h}{2}} \sigma x\, dx$$

$$= 2\int_0^{\frac{g}{2}} E\epsilon_{max}\frac{2x}{h}x\, dx + 2\int_{\frac{g}{2}}^{\frac{h}{2}}\{(E - H)\epsilon_y + H\epsilon_{max}\frac{2x}{h}\}x\, dx$$

At initial yield $M_y = E\epsilon_y h^2/6$ so the integral becomes:

$$\frac{M}{M_y} = \frac{1}{2}(1 - \frac{H}{E})(3 - \frac{\epsilon_y^2}{\epsilon_{max}^2}) + \frac{H}{E}\frac{\epsilon_{max}}{\epsilon_y} \tag{28}$$

Bending and Stretching of Curved Bar

Geometry of Deformation

A small segment $d\phi$ of a rectangular bar with circular centreline is shown in Figure 15, and the following geometrical relations apply:

$$\text{Total rotation of face} \qquad \omega = d\alpha + \bar{\epsilon}d\phi \tag{29}$$

where ϵ is uniform strain, $d\alpha$ is rotation, so:

$$\frac{d\omega}{d\phi} = \frac{d\alpha}{d\phi} + \bar{\epsilon} = \beta + \bar{\epsilon} \tag{30}$$

Rotation of the bar centreline is greater by the increase of shear deflection from γ to $\gamma + d\gamma$, so the equation for change of curvature is:

$$r_0\{d\phi(1 + \epsilon) + d\alpha + d\gamma\} = \bar{r}d\phi(1 + \bar{\epsilon})$$

so since $\bar{\epsilon}$ is small:

$$\frac{1}{r} - \frac{1}{r_0} = \frac{1}{\bar{r}(1 + \epsilon)}(\beta + \frac{d\gamma}{d\phi})$$

$$= \frac{1}{\bar{r}}(1 - \epsilon)(\beta + \frac{d\gamma}{d\phi}) \tag{31}$$

Stresses and Strains

$$\text{Fibre strain} \qquad \epsilon = \frac{r\epsilon d\phi + (r - \bar{r})d\alpha}{rd\phi}$$

$$= \epsilon + \beta(1 - \frac{\bar{r}}{r}) \tag{32}$$

Yield in tension and compression occurs where $\epsilon = \pm \epsilon_y$, with corresponding radii:

$$\left.\begin{array}{c} r_c \\ r_t \end{array}\right\} = \frac{\beta \bar{r}}{\beta + \epsilon \pm \epsilon_y} \tag{33}$$

Fibre stresses are found with equations (26) and (27):

$$\text{Elastic region} \quad r_c \le r \le r_t \qquad \sigma = E\epsilon$$

$$= E\{\epsilon + \beta(1 - \frac{\bar{r}}{r})\} \tag{34}$$

Plastic region, assuming $r_t > r_c$:

$$\begin{array}{l} \text{Tension} \quad r > r_t \\ \text{Compression} \quad r < r_c \end{array} \qquad \sigma = \pm(E - H)\epsilon_y + H(\epsilon + \beta) - H\beta\frac{\bar{r}}{r} \tag{35}$$

Force and moment per unit width are found by integrating stress over the cross section, using the appropriate equation for elastic or plastic stress regions.

$$F = \int_{r_1}^{r_2} \sigma \, dr \tag{36}$$

$$M = \int_{r_1}^{r_2} \sigma \, r dr \tag{37}$$

Explicit integrals for radius limits a, b, can be found from expressions (34) or (35):

$$\text{Elastic Region} \quad \text{Forces} \qquad F = E[(\beta + \epsilon)r - \beta\bar{r}\log_e r]_a^b \tag{38}$$

$$\text{Elastic Region} \quad \text{Moments} \qquad M = E[(\beta + \epsilon)r^2/2 - \beta\bar{r}r]_a^b \tag{39}$$

$$\text{Plastic Region} \quad \text{Forces} \qquad F = \left[\{\pm(E - H)\epsilon_y + H(\beta + \epsilon)\}r - H\beta\bar{r}\log_e r\right]_a^b \tag{40}$$

$$\text{Plastic Region} \quad \text{Moments} \qquad M = \left[\{\pm(E - H)\epsilon_y + H(\beta + \epsilon)\}r^2/2 - H\beta\bar{r}r\right]_a^b \tag{41}$$

Using radius limits found from equation (33), values of F and M for given β and ϵ can be found from equations (38) - (41). To find β and ϵ as functions of F and M requires solution of nonlinear simultaneous equations. Since the diagonal terms predominate (F is principally a function of ϵ and M of β), simple linear inverse interpolation can be used. (A Newton-Raphson solution was first programmed but was not necessary.)

Pure Bending of Curved Bar

Shear is zero, and for each value of β, a value of $\bar{\epsilon}$ is found giving no net force ($F = 0$). The resultant value of M is expressed in the form:

$$M/M_y = f(\beta/\beta_y) \tag{42}$$

where M_y, β_y are values of moment and rotation at initial yield (at the intrados).

Circular Proving Ring

For symmetrical loading, the ring can be represented by one quadrant (Fig. 16). Forces and moments at angle ϕ for load $2P$ are:

$$\text{Normal Force} \quad F = P\cos\phi \tag{43}$$

$$\text{Shear Force} \quad V = -P\sin\phi \tag{44}$$

$$\text{Moment} \quad M = M_0 + P\bar{r}\cos\phi \tag{45}$$

Deflection Equations

(i) Rotation

Symmetry requires a boundary condition such that there is no net rotation over the quadrant:

$$\int_0^{\frac{\pi}{2}} \frac{d\omega}{d\phi}d\phi = \int_0^{\frac{\pi}{2}} (\beta + \bar{\epsilon})d\phi = 0 \tag{46}$$

The value of M_0 for given P can be found when this integral is satisfied.

(ii) Centreline Deflection of Ring

Geometry of deformed ring is shown in Figure 17, and neglecting second order terms:

$$\text{Initial curvature} \quad \frac{1}{\bar{r}} = \frac{d\phi}{ds}$$

$$\text{Deflected curvature} \quad \frac{1}{r_1} = \frac{d\phi + \Delta\,d\phi}{ds + \Delta\,ds} = \frac{d\phi + \dfrac{d^2u}{ds^2}ds}{ds\,(1 - u/\bar{r})}$$

$$\text{Change in curvature} \quad \frac{1}{r_1} - \frac{1}{\bar{r}} = \frac{\dfrac{1}{\bar{r}} + \dfrac{d^2u}{ds^2}}{1 - u/\bar{r}} - \frac{1}{\bar{r}}$$

$$= \frac{1}{\bar{r}^2}\Big(\frac{d^2u}{d\phi^2} + u\Big) \tag{47}$$

Using equation (31), and noting that opposite sense of M in Figures 15 and 16 reverses signs, the differential equation for deflection becomes:

$$\frac{1}{\bar{r}^2}\Big(\frac{d^2u}{d\phi^2} + u\Big) = \frac{1}{\bar{r}}(1 - \bar{\epsilon})\Big(\beta + \frac{d\gamma}{d\phi}\Big)$$

$$\frac{d^2u}{d\phi^2} + u = \bar{r}(1 - \bar{\epsilon})\Big(\beta + \frac{d\gamma}{d\phi}\Big) \tag{48}$$

Shear deflection γ is small and is assumed equal to the elastic deflection:

$$\gamma = \frac{\kappa V}{GA}$$

where κ is the shape coefficient for shear and A cross-sectional area. Substituting V from equation (44):

$$\frac{d\gamma}{d\phi} \approx -\frac{\kappa P\cos\phi}{GA} \tag{49}$$

so the deflection equation becomes:

$$\frac{d^2u}{d\phi^2} + u = \bar{r}(1 - \epsilon)\Big(\beta - \frac{\kappa P\cos\phi}{GA}\Big) \tag{50}$$

The differential equation (50) is integrated using any standard numerical integration technique, with terms $\bar{\epsilon}$ and β for each angle ϕ calculated as previously indicated.

APPENDIX B – MODIFICATIONS TO PAFEC CODE

The modifications listed were applied to PAFEC plasticity code at level 5.2. It is expected[17] that later releases of PAFEC will include these or similar modifications having the same effect.

(i) **Damping.** When oscillatory behaviour occurs and convergence is uncertain, a damping routine may be invoked. This may lead to incorrect implementation of the Prandtl-Reuss equations and has been discarded. Section (iii) describes other means used for securing convergence.

(ii) **Kinematic Hardening.** Implementation of the Prandtl-Reuss equations has been modified to properly incorporate yield surface translation.

(iii) **Convergence.** Convergence is accelerated and stability improved by adaptive adjustment of a convergence parameter.

    (a) Convergence is accelerated when too slow.

    (b) When maximum error increases (instability), previous converged values are restored and convergence slowed until error reduces.

    (c) After convergence is re-established, it is again accelerated to hasten attainment of solution within tolerance.

(iv) **Iteration Loop.** Exit conditions have been changed so that a self-correcting load adjustment[18] is applied at the start of the next load increment. This greatly improves solution accuracy for given error tolerance, and may allow tolerance level to be relaxed while maintaining satisfactory accuracy.

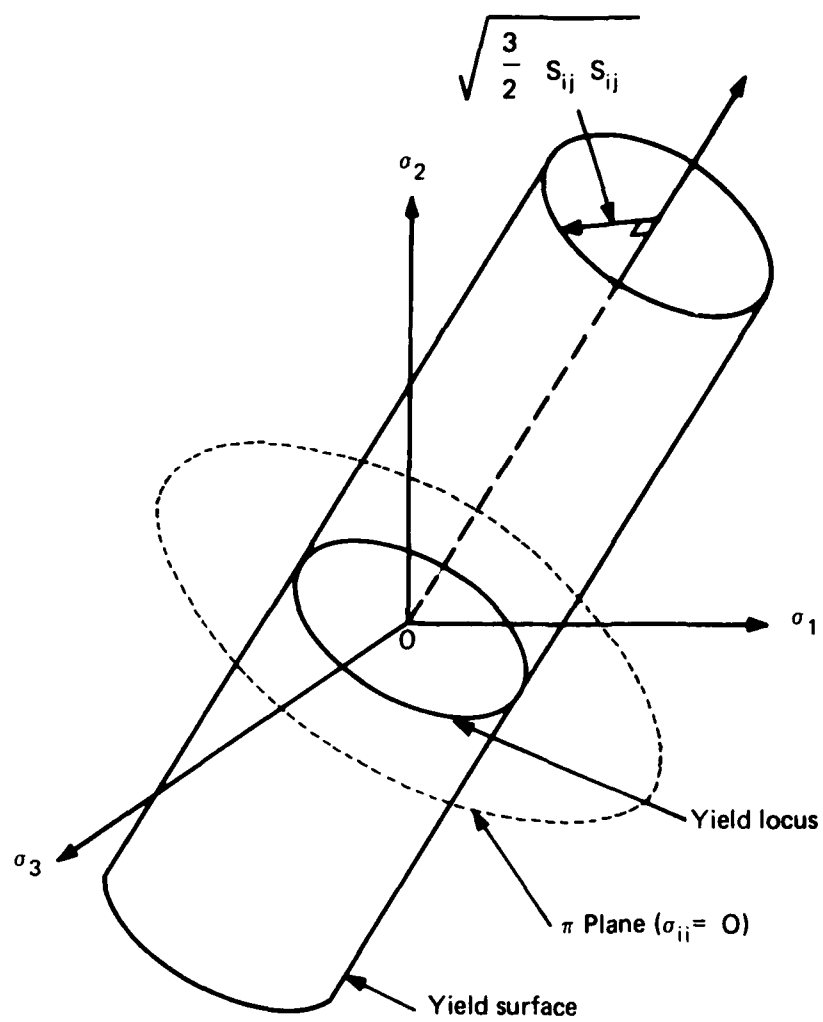(v) **Mixed Hardening.** Mixed kinematic-isotropic hardening with variable proportioning has been included.

$$\sqrt{\frac{3}{2}\, S_{ij}\, S_{ij}}$$

σ_2

σ_1

σ_3

0

Yield locus

π Plane ($\sigma_{ii} = 0$)

Yield surface

FIG. 1   REPRESENTATION OF VON MISES YIELD SURFACE

Kinematic hardening
(showing Bauschinger effect)

Mixed hardening

Isotropic hardening
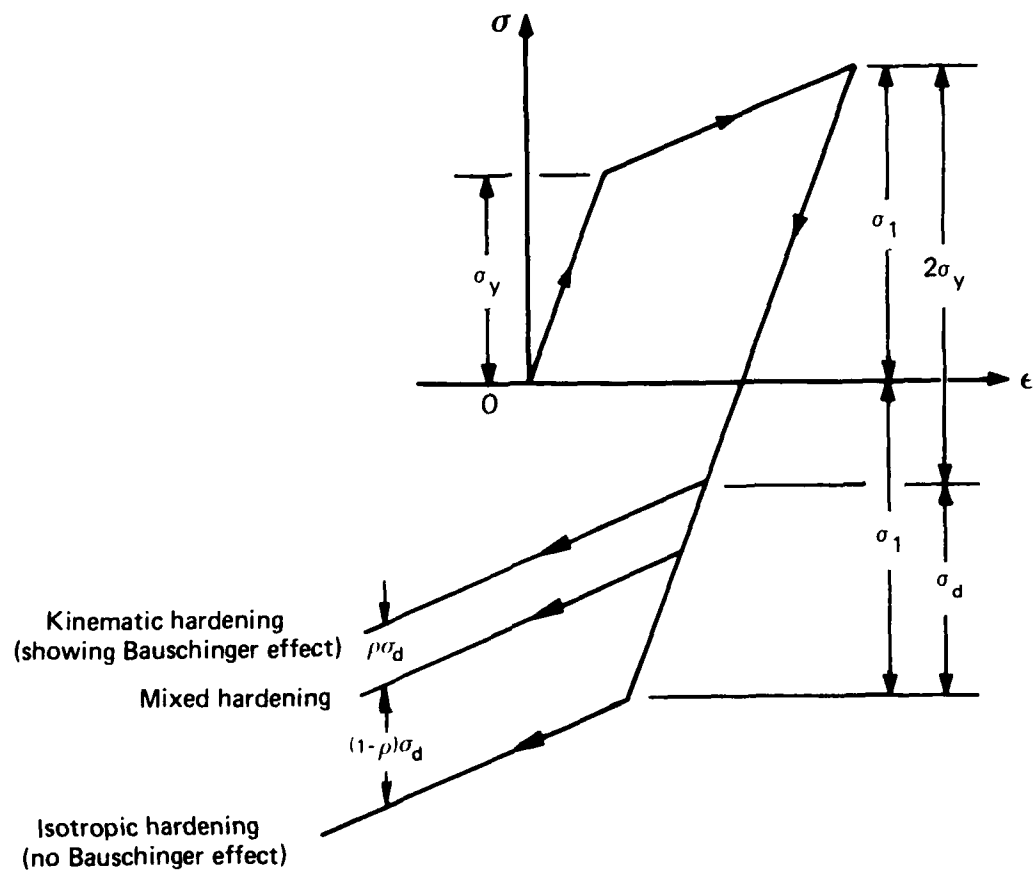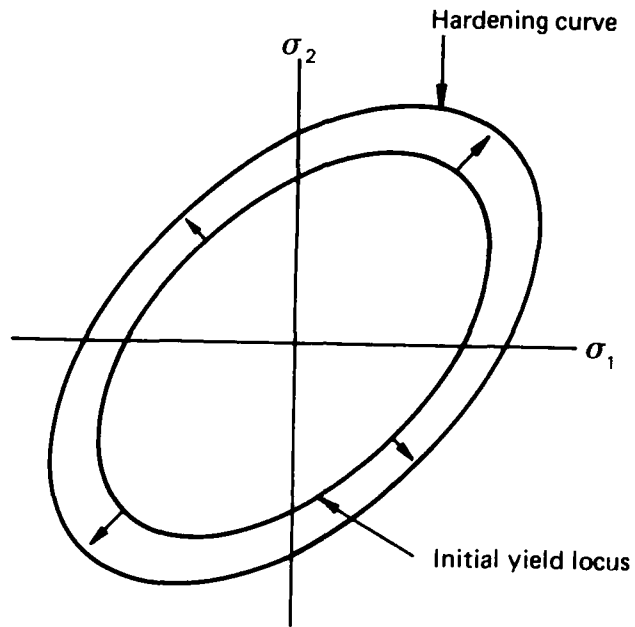(no Bauschinger effect)

FIG. 2   STRAIN HARDENING BEHAVIOUR

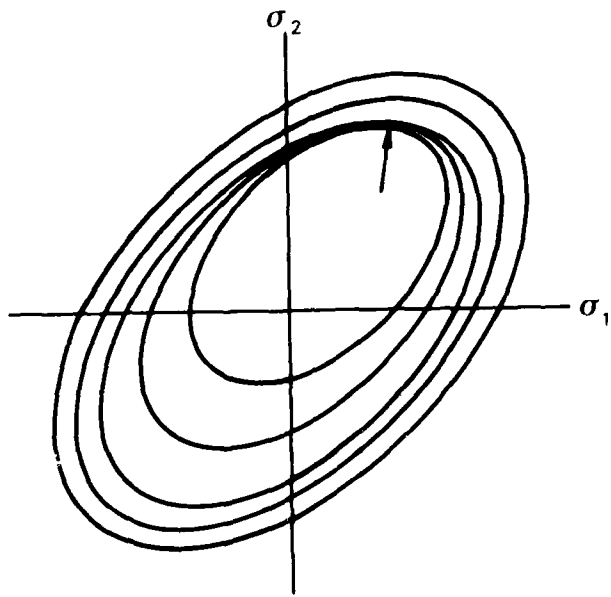FIG. 3   ISOTROPIC HARDENING
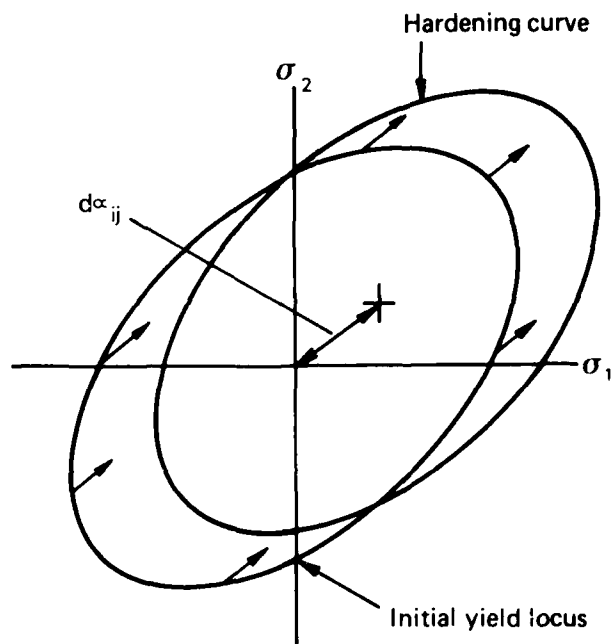
FIG. 4   KINEMATIC HARDENING
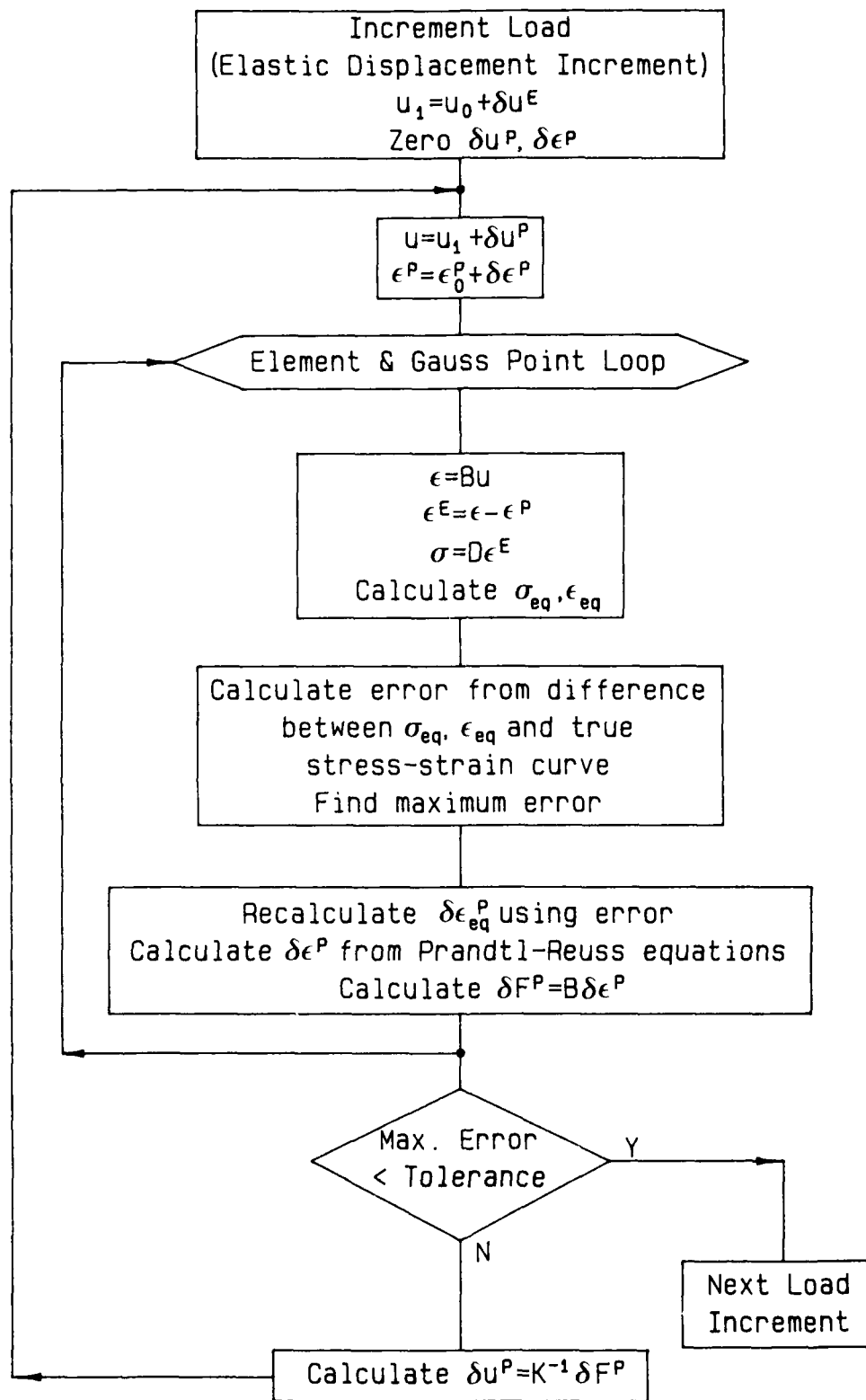
FIG. 5   MROZ HARDENING

Increment Load
(Elastic Displacement Increment)
$$u_1 = u_0 + \delta u^E$$
Zero δu^P, $\delta \epsilon^P$

$$u = u_1 + \delta u^P$$
$$\epsilon^P = \epsilon_0^P + \delta \epsilon^P$$

Element & Gauss Point Loop

$$\epsilon = Bu$$
$$\epsilon^E = \epsilon - \epsilon^P$$
$$\sigma = D\epsilon^E$$
Calculate σ_{eq}, ϵ_{eq}

Calculate error from difference
between σ_{eq}, ϵ_{eq} and true
stress-strain curve
Find maximum error

Recalculate $\delta \epsilon_{eq}^P$ using error
Calculate $\delta \epsilon^P$ from Prandtl-Reuss equations
Calculate $\delta F^P = B \delta \epsilon^P$

Max. Error
< Tolerance

Y

N

Next Load
Increment

Calculate $\delta u^P = K^{-1} \delta F^P$

FIG. 6   PAFEC PLASTICITY ALGORITHM

E = 85.9 GPa
v = 0.3237
σ_y = 189 MPa
H = 3160 MPa

Thickness 0.0127m

0.178m

0.127m
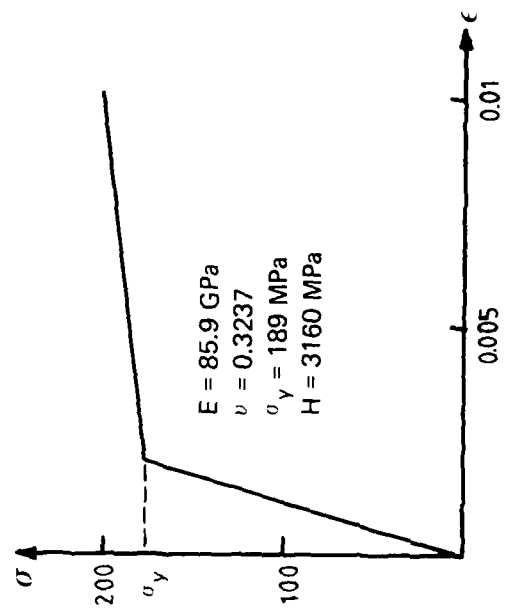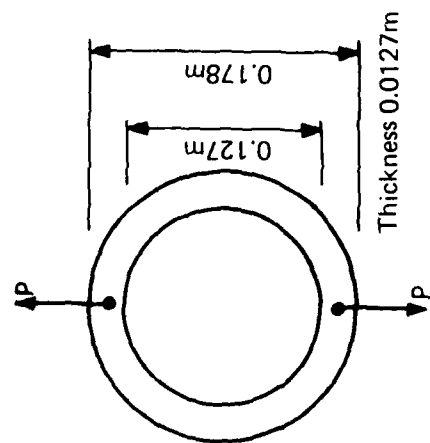
FIG. 7   PROVING RING – DIMENSIONS AND PROPERTIES
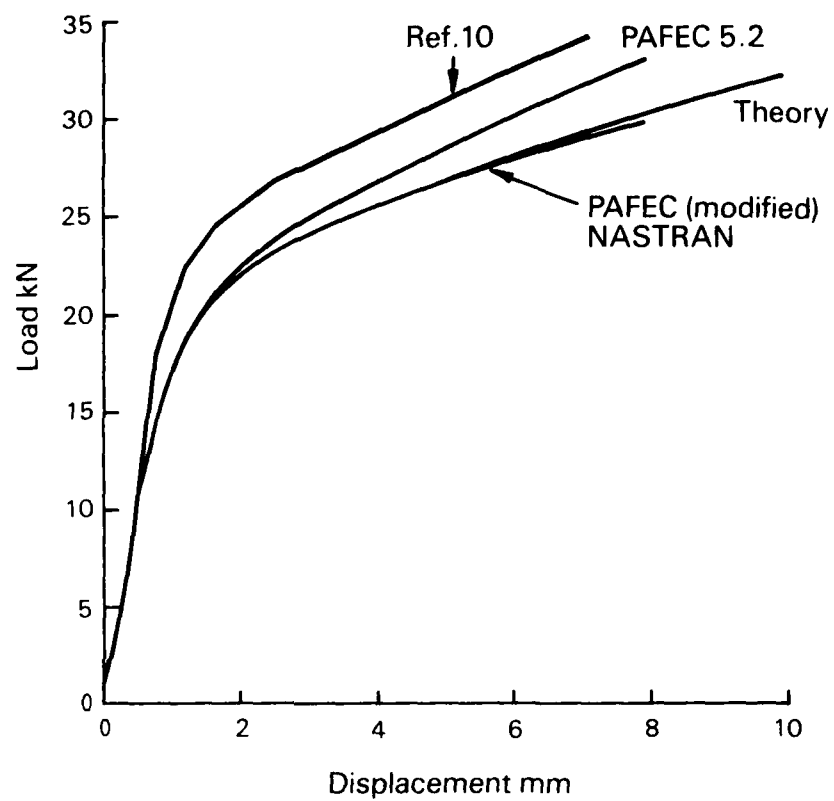
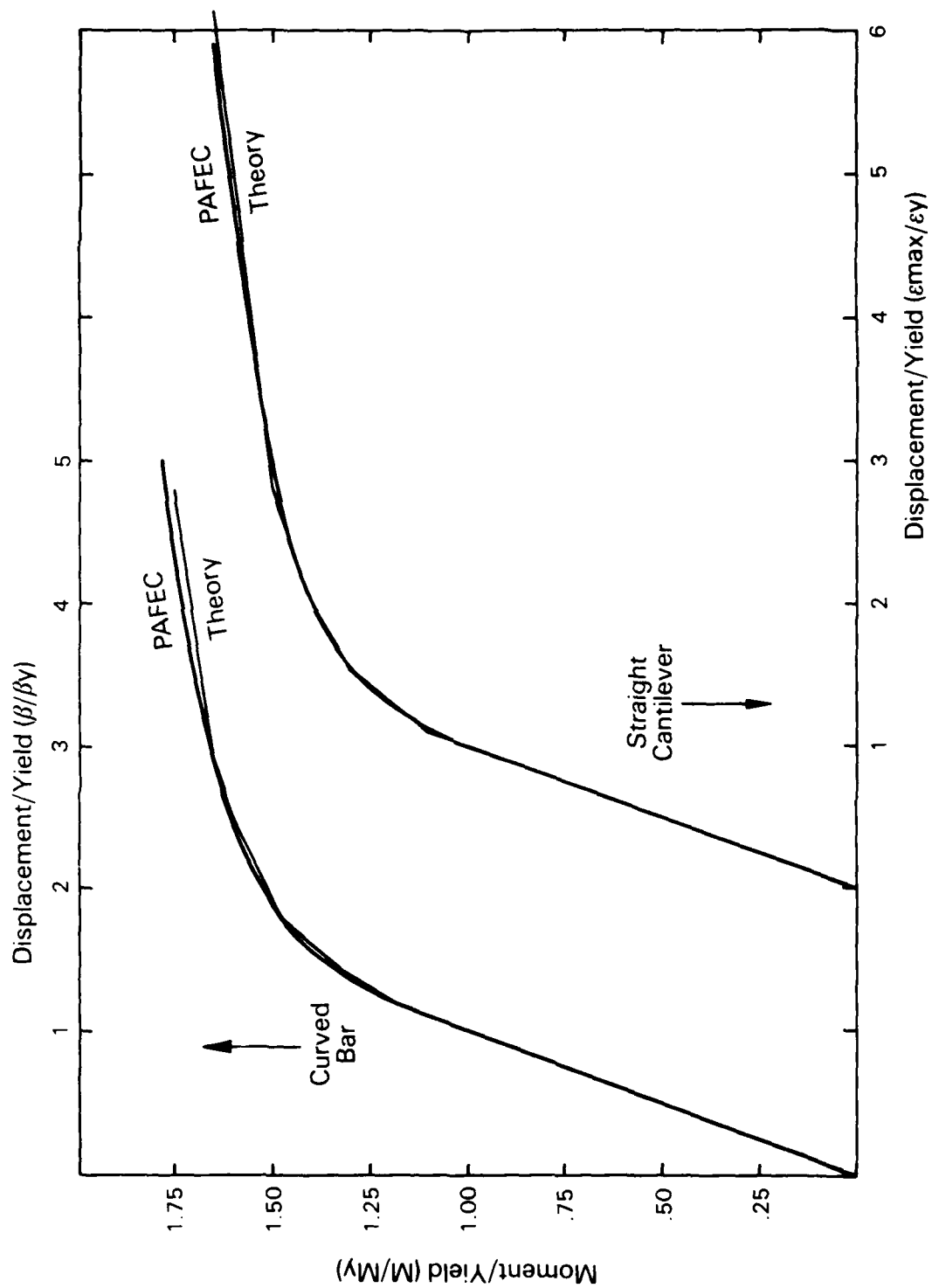FIG. 8   COMPARISON OF SOLUTIONS FOR PROVING RING (SEE FIG. 7)

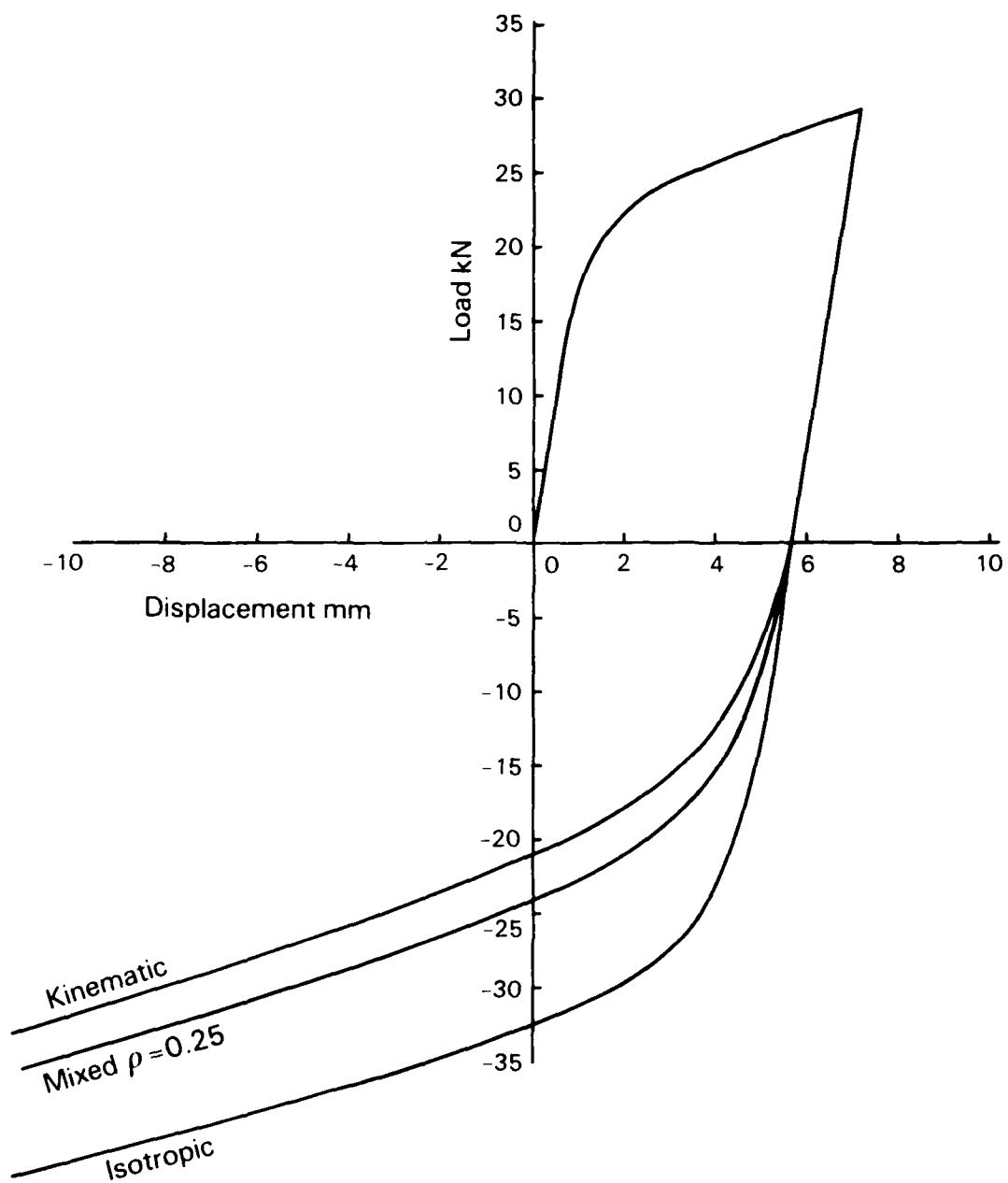FIG. 9   STRAIGHT CANTILEVER AND CURVED BAR IN PURE BENDING

FIG. 10   CYCLIC LOADING OF PROVING RING

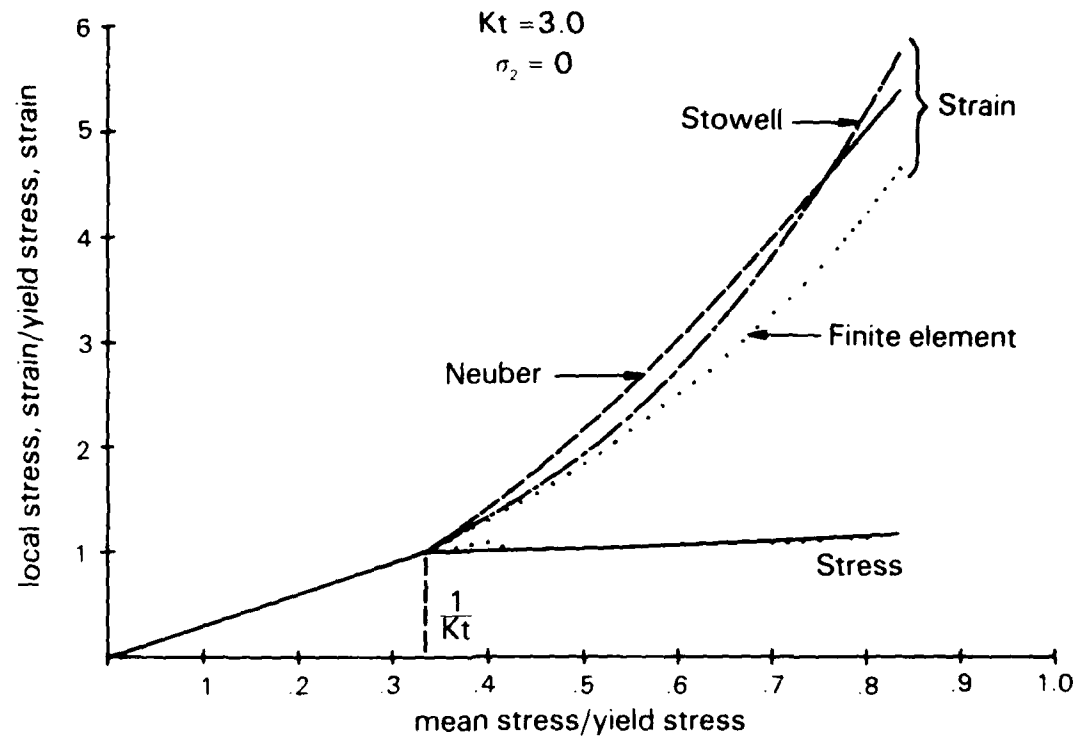PLASTIC STRESS/STRAIN CONCENTRATIONS
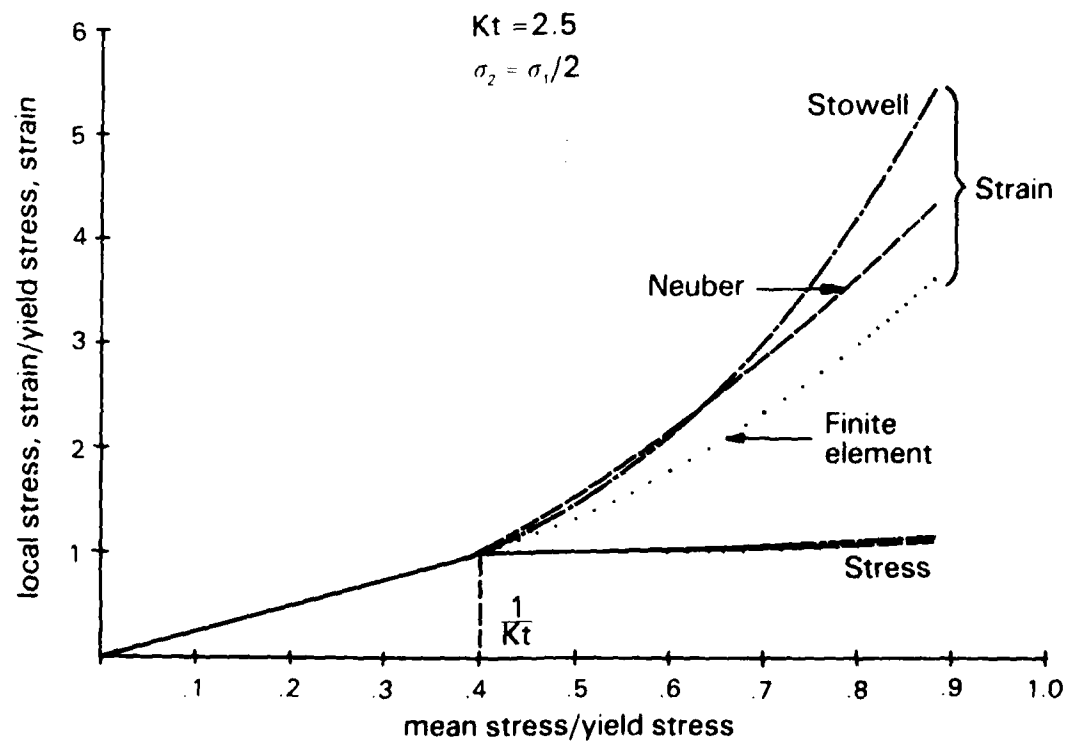

FIG. 11   HOLE IN PLATE — UNIAXIAL STRESSES

FIG. 12   HOLE IN PLATE — PARTIAL BIAXIAL STRESS

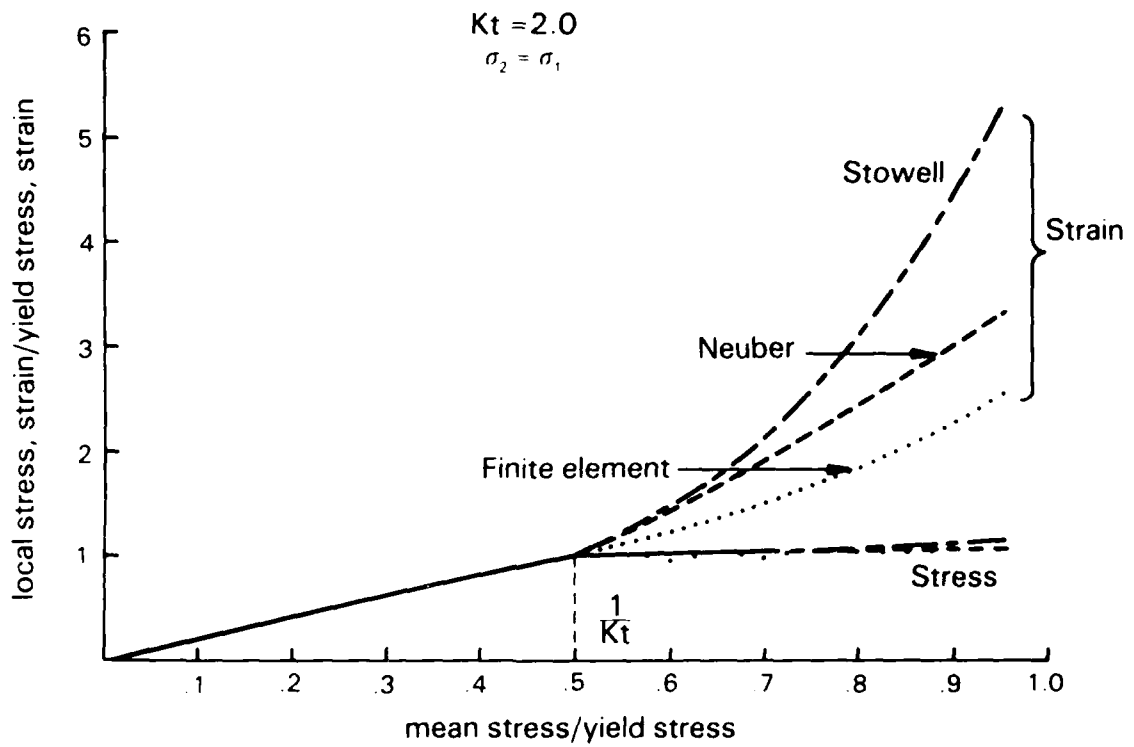# PLASTIC STRESS/STRAIN CONCENTRATIONS

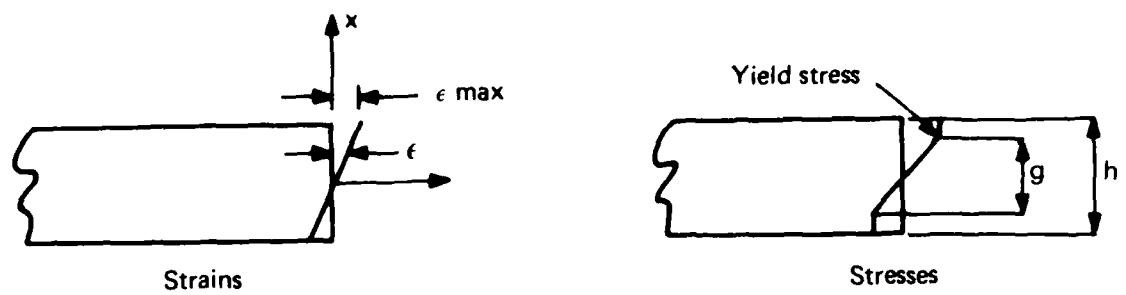FIG. 13   HOLE IN PLATE BIAXIAL STRESSES
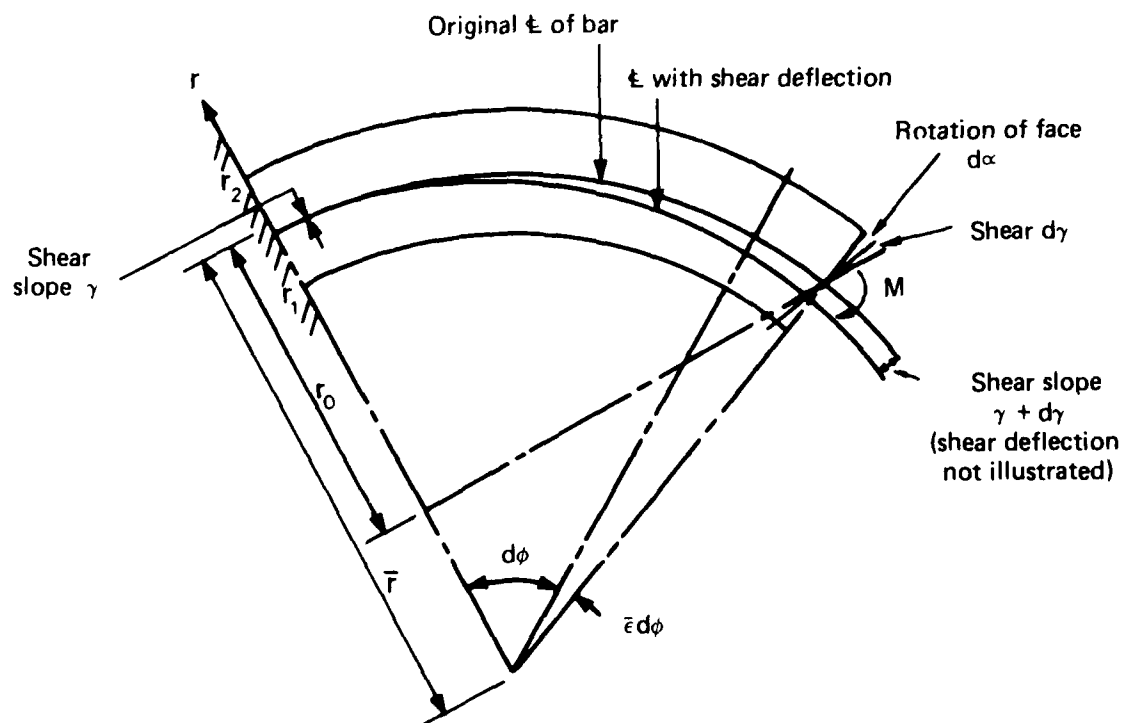
FIG. 14   RECTANGULAR BAR – STRESSES AND STRAINS

FIG. 15   CURVED BAR – DEFLECTION AND STRAIN

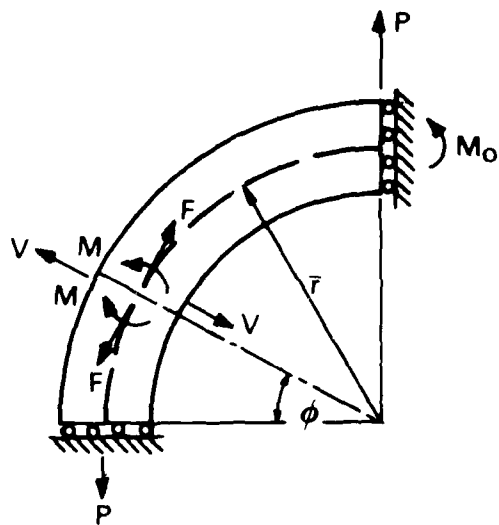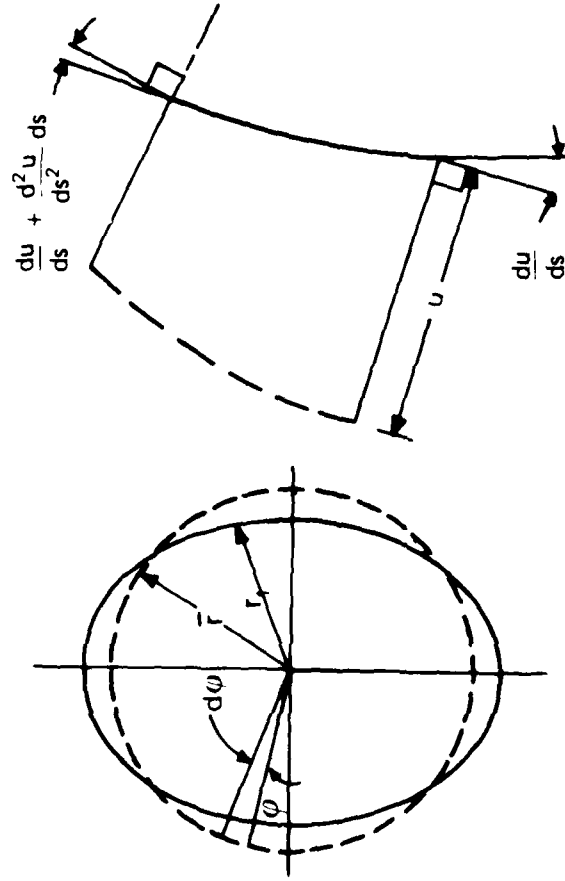FIG. 16   PROVING RING – LOADING

FIG. 17   CURVED BAR – DEFLECTION OF CENTRELINE

DISTRIBUTION

AUSTRALIA

Department of Defence

Defence Central
Chief Defence Scientist
Deputy Chief Defence Scientist (shared copy)
Superintendent, Science and Program Administration (shared copy)
Controller, External Relations, Projects and
    Analytical Studies (shared copy)
Director, Departmental Publications
Counsellor, Defence Science (London) (Doc Data Sheet Only)
Counsellor, Defence Science (Washington) (Doc Data Sheet Only)
Scientific Adviser to the Thailand Military Research and Development
    Centre
Defence Central Library
Document Exchange Centre, DISB (18 copies)
Joint Intelligence Organisation
Librarian H Block, Victoria Barracks, Melbourne
Director General - Army Development (NSO) (4 copies)
Defence Industry and Materiel Policy, FAS

Aeronautical Research Laboratories
Director
Library
Superintendent - Aero Propulsion
Divisional File - Aero Propulsion
Author: N. S. Swansson

Materials Research Laboratories
Director/Library

Defence Research Centre
Library

RAN Research Laboratory
Library

Navy Office
Navy Scientific Adviser
Director of Naval Aircraft Engineering
Director of Naval Ship Design

Army Office
Scientific Adviser - Army
Engineering Development Establishment, Library
Royal Military College, Library
US Army Research, Development and Standardisation Group

Air Force Office
Air Force Scientific Adviser
Aircraft Research and Development Unit
    Scientific Flight Group
    Library
Technical Division Library

Director General Aircraft Engineering - Air Force
RAAF College, Point Cook

Central Studies Establishment
Information Centre

Government Aircraft Factories
Library

Department of Aviation
Library

Statutory and State Authorities and Industry
Australian Atomic Energy Commission, Director
Gas & Fuel Corporation of Vic., Manager Scientific Services
SEC of Vic., Herman Research Laboratory, Library
BHP, Melbourne Research Laboratories
Hawker de Havilland Aust Pty Ltd, Bankstown, Library
Hawker de Havilland Aust Pty Ltd, Victoria, Library

Universities and Colleges
Adelaide
Barr Smith Library

Melbourne
Engineering Library

Monash
Hargrave Library

Newcastle
Library

New England
Library

Sydney
Engineering Library

NSW
Physical Sciences Library
Library, Australian Defence Force Academy

Queensland
Library

Tasmania
Engineering Library

Western Australia
Library

RMIT
Library

CANADA
　　CAARC Coordinator Structures
　　Energy Mines & Resources Dept
　　　Physics and Metallurgy Research Laboratories
　　NRC
　　　Aeronautical & Mechanical Engineering Library
　　　Division of Mechanical Engineering, Director
　　Pratt & Whitney Canada

　　Universities and Colleges
　　　Toronto
　　　　Institute for Aerospace Studies

FRANCE
　　ONERA, Library

GERMANY
　　Fachinformationszentrum: Energie, Physic, Mathematik GMBH

INDIA
　　CAARC Coordinator Structures
　　Defence Ministry, Aero Development Establishment, Library
　　Gas Turbine Research Establishment, Director
　　National Aeronautical Laboratory, Information Centre

ISRAEL
　　Technion-Israel Institute of Technology
　　　Professor J. Singer

ITALY
　　Professor Ing. Guiseppe Gabrielli

JAPAN
　　National Aerospace Laboratory
　　Institute of Space and Astronautical Science, Library

　　Universities
　　　Kagawa University
　　　　Library

NETHERLANDS
　　National Aerospace Laboratory (NLR), Library

NEW ZEALAND
　　CAARC Coordinator Propulsion
　　Defence Scientific Establishment, Library

　　Universities
　　　Canterbury
　　　　Library

SWEDEN
　　Aeronautical Research Institute, Library
　　Swedish National Defense Research Institute (FOA)

UNITED KINGDOM

Ministry of Defence, Research, Materials and Collaboration
CAARC, Secretary
CAARC Coordinator Propulsion
Royal Aircraft Establishment
    Pyestock, Director
    Farnborough, Library
Admiralty Research Establishment
    Holton Heath, Dr N.J. Wadsworth
    St Leonard's Hill, Superintendent
National Engineering Laboratory, Library
British Library, Document Supply Centre
CAARC Co-ordinator, Structures
Aircraft Research Association, Library
British Maritime Technology Ltd
Electrical Power Engineering Company Ltd
GEC Gas Turbines Ltd, Managing Director
Fulmer Research Institute Ltd, Research Director
Rolls-Royce Ltd, Aero Division Bristol, Library
Welding Institute, Library
British Aerospace
    Kingston-upon-Thames, Library
    Hatfield-Chester Division, Library
British Hovercraft Corporation Ltd, Library

Universitites & Colleges
Bristol
    Engineering Library

Cambridge
    Library, Engineering Department
    Whittle Library

London
    Library

Manchester
    Library

Nottingham
    Science Library

Southampton
    Library

Liverpool
    Library

Strathclyde
    Library

Cranfield Inst. of Technology
    Library

Imperial College
    Aeronautics Library

UNITED STATES OF AMERICA
Air Force Wright Aeronautical Laboratories, Library
Naval Air Propulsion Center, Library
NASA Scientific and Technical Information Facility
Materials Information, American Society for Metals
Allis Chalmers Corporation, Library
Avco Lycoming Stratford Division
Boeing Company, Library
General Electric Co. Aircraft Engine Group
Pratt & Whitney
United Technologies Corporation, Library
Lockheed - California Company
Lockheed Missiles and Space Company
Lockheed Georgia
McDonnell Aircraft Company, Library

Universities and Colleges
Chicago
John Crerar Library

Florida
Aero Engineering Department

Johns Hopkins
Library

Iowa State
Library

Iowa
Library

Princeton
Library

Massachusetts Inst. of Tech.
MIT Libraries

SPARES (10 copies)
TOTAL (156 copies)

1.a. AR No. AR-004-512	1.b. Establishment No ARL-AERO-PROP-R-174	2. Document Date DECEMBER 1986	3. Task No DST/86040
4. Title APPLICATION OF FINITE ELEMENT METHODS WITH CYCLIC ELASTO-PLASTIC ANALYSIS TO LOW CYCLE FATIGUE ANALYSIS OF ENGINE COMPONENTS		5. Security a. document UNCLASS	6. No Pages 34
		b. title c. abstract U U	7. No Refs 27
8. Author(s) N.S. SWANSSON		9. Downgrading Instructions	
10. Corporate Author and Address Aeronautical Research Laboratories P.O. Box 4331, MELBOURNE, VIC. 3001		11. Authority (as appropriate) a.Sponsor b.Security c.Downgrading d.Approval	

12. Secondary Distribution (of this document)

Approved for public release.

Overseas enquirers outside stated limitations should be referred through ASDIS, Defence Information Services Branch, Department of Defence, Campbell Park, CANBERRA ACT 2601

13.a. This document may be ANNOUNCED in catalogues and awareness services available to ...

No limitations

13.b. Citation for other purposes (ie casual announcement) may be (select) unrestricted(or) as for 13 a.

14. Descriptions	15. COSATI Group
Finite element analysis Elastic-plastic analysis Biaxial stresses Stress concentration	11130 21100

16. Abstract

     Low Cycle Fatigue (LCF) in engine components involves macroscopic cyclic plastic strains (with a stress-strain hysteresis loop) over a significant portion of the failure region. Characterising elasto-plastic behaviour in potential failure regions is a necessary step in estimating LCF life.

     The equations governing elasto-plastic behaviour are summarized, and the methods of implementing them in Finite Element (FE) stress analysis programs discussed.

     An extension of the PAFEC program to include mixed isotropic-kinematic hardening is outlined, and verified by examples for which alternative FE solutions were available.

16. Abstract (contd)

A sample application has been made to holes in a plate with biaxial stress fields similar to those in disc webs, and the results compared with the Neuber and modified Stowell rules commonly used for design life estimation; these rules tend to overestimate the strain in biaxial stress conditions, leading to conservative life estimates.

17. Imprint

Aeronautical Research Laboratories, Melbourne

18. Document Series and Number	19. Cost Code	20. Type of Report and Period Covered
AERO PROPULSION REPORT 174	41 3151	

21. Computer Programs Used

PAFEC
NASTRAN

22. Establishment File Ref(s)

M2/645

FILMED
48